CrystEngComm

Accepted Manuscript

ROYAL SOCIETY OF CHEMISTRY

www.rsc.org/crystengcomm

Mesoporous CeO_2 nanoparticles assembled by hollow nanostructures: formation mechanism and enhanced catalytic property

Jingcai Zhang[a], Hongxiao Yang[b], Shuping Wang[a], Wei Liu[a], Xiufang Liu[a], Jinxin Guo*[a] and Yanzhao Yang*[a]

[a] *Key Laboratory for Special Functional Aggregate Materials of Education Ministry, School of Chemistry and Chemical Engineering, Shandong University, Jinan, 250100, P. R. China. Fax: +86-531-88564464; Tel: +86-531-88362988; E-mail: yzhyang@sdu.edu.cn; E-mail: jinxinguo@sdu.edu.cn.*

[b] *School of Chemistry and Chemical Engineering, University of Jinan, Jinan, Shandong 250022, People's Republic of China*

** Corresponding author*

Received (in XXX, XXX) Xth XXXXXXXXX 20XX, Accepted Xth XXXXXXXXX 20XX

DOI: 10.1039/b000000x

In this paper, a novel hierarchically mesoporous CeO_2 nanoparticles assembled by hollow nanocones have been prepared through a facile solvothermal strategy using $Ce(HCOO)_3$ as the precursor. X-ray diffraction (XRD), transmission electron microscopy (TEM), high resolution transmission electron microscopy (HRTEM), field-emission scanning electron microscope (FE-SEM) and thermal gravimetric analysis (TGA) were utilized to characterize the products and research the formation mechanism. The whole synthesis process involves two steps: the formation of $Ce(HCOO)_3$ nanoparticles constructed with nanocones at room temperature in an alkaline environment and oxidation induced phase transformation from $Ce(HCOO)_3$ to CeO_2 with the formation of hollow nanocones assembled by nanocrystals in the solvothermal process at 150 ^oC. The as-prepared mesoporous CeO_2 nanoparticles with the average diameter of 500 nm displayed a high surface area of 147.6 $m^2\ g^{-1}$ by N_2 adsorption and desorption measurement. The H_2-TPR test showed its great reduction behavior in low temperature zone. By comparing the T100 temperature of CO conversion with commercial sample (above 350 ^oC) and other reported samples (above 300 ^oC) in the literatures, the mesoporous CeO_2 nanoparticles (270 ^oC) presented an excellent catalytic activity for CO oxidation.

Introduction

Hierarchically nanostructured materials have attracted considerable interest due to their enhanced properties and potential applications.[1-8] Up to now, a wealth of methods has been used for controlled synthesis of hierarchically nanostructured materials[9], such as precursor template synthesis,[10] ionic liquid assisted route,[11] hydrothermal/solvothermal synthesis.[12,13] For example, 3D-hierarchical Cu_3SnS_4 flowerlike microspheres have been successfully synthesized through a solvothermal process and the obtained Cu_3SnS_4 photocatalysts without any loadings exhibit good photocatalytic activity.[14] Novel hierarchical flower-like Bi_2MoO_6 hollow spheres constructed with nanoflakes have been fabricated via a facile template-free solvothermal process in the presence of ethylene glycol.[15]

As an important functional inorganic material, ceria has been under extensive investigation for its various applications in catalysis,[16] chemical mechanical polishing materials,[17] fuel cells,[18] oxygen sensors[19] and UV blockers.[20] Especially, many endeavors have been devoted to investigate the catalytic performances of the ceria-based nanomaterials. For example, Tang's group studied the remarkably enhanced catalytic activity of core-shell Au@CeO_2 nanocoposites for CO oxidation and the superior photocatalysts of multi-shelled CeO_2 hollow microspheres for water oxidation in details.[21, 22] The large contact areas and the mesopores promoted the catalytic oxidation of CO, while the triple-shelled hollow structure, the larger surface area and the more curved surfaces of the TSCeHSs enhanced the photocatalytic oxidation of water. To date, considerable efforts have been focused on the fabrication of CeO_2 3D hierarchical structures constructed with nanoparticles, nanorods, nanoflakes, due to their enhanced properties.[23-26] For example, Jeong's group synthesized CeO_2 with flowerlike microstructure through a cerium-based coordination polymers with a calcination process, later La_2O_3 and Gd_2O_3 were fabricated by the same method.[27] Sun et al. fabricated nearly monodisperse flowerlike CeO_2 microspheres via the calcination of a $Ce(OH)CO_3$ precursor and the as-prepared CeO_2 decorated with Cu showed excellent catalytic properties and marked hydrothermal stability for ethanol steam reforming.[28] Without calcinations process, Sato's group prepared 3D flowerlike CeO_2 under subcritical and supercritical temperature of 350-380 ^oC via a solvothermal process and the as-formed flowerlike CeO_2 decorated with 5% Gd displays higher catalytic activity than pure CeO_2 for CO oxidation.[29] However, these methods conventionally require either rigorous conditions or high temperature.

Recently, our research group has been focused on fabrication of CeO_2 with satisfactory structure in a mild solution route.[30-33] We have reported a simple solvothermal method to obtain $Ce(HCOO)_3$, followed by annealing the $Ce(HCOO)_3$ at high temperature to obtain CeO_2 three dimensional micro/nanostructures.[30] Based on this work, we had designed a one-step and facile strategy to synthesize mesoporous CeO_2 nanoflowers derived from $Ce(HCOO)_3$ and $Ce_2(C_2O_4)_3{\cdot}10H_2O$ through a solvothermal or hydrothermal route.[31, 32] Even though we have reported self-assembly of ceria nanocrystals starting from $Ce(HCOO)_3$ in the neutral condition.[31] In our current work, we synthesized a novel hierarchically mesoporous CeO_2 nanoparticles assembled by hollow nanocones derived from $Ce(HCOO)_3$ under the changed experiment condition and studied

the formation mechanism in detail. It is worth mentioning that there were few reports about the mesoporous hollow cone-like structure according to our knowledge. The whole process involved two steps: 1. the preparation of the $Ce(HCOO)_3$ nanoparticles constructed with nanocones in a short time in an alkaline environment at room temperature; 2. the transformation from $Ce(HCOO)_3$ to CeO_2 with the formation of hollow nanocones by the oxidation of H_2O_2 in the solvothermal process. The final product displayed a high surface area of 147.6 m^2 g^{-1} and excellent catalytic activity for CO oxidation.

Experimental Section

Materials

All the reactants were analytical grade and used without further purification. Cerium(III) nitrate hexa-hydrate [$Ce(NO_3)_3{\cdot}6H_2O$, >99.0%] and cerium(IV) oxide powders (CeO_2, >99.0%) were purchased from Tianjin Kemiou Chemical Reagent Co. Ltd. Formic acid (HCOOH, >88.0 %), Polyoxyethylene(10) octylphenyl ether (OP-10, 99.0%), hydrogen peroxide (H_2O_2, 30 %), and the ammonia solution ($NH_3{\cdot}H_2O$, 25 %) were obtained from Sinopharm Chemical Reagent Co. Ltd. $NH_3{\cdot}H_2O$ solution with a concentration of 10 M was obtained by diluting commercial ammonia solution ($NH_3{\cdot}H_2O$, 25%). Deionized water and absolute alcohol were used throughout.

Synthesis of CeO_2 nanoparticles

In a typical procedure, 0.117 g (0.27 mmol) $Ce(NO_3)_3{\cdot}6H_2O$ was dissolved in 15 mL of absolute alcohol under vigorous stirring, then 130 µL OP-10 and 100 µL HCOOH was added. Subsequently, a white colloidal solution was obtained immediately after the rapid addition of 500 µL 10 M $NH_3{\cdot}H_2O$. After continuous stirring for 20 min, the color of the colloidal solution turned to brown with the addition of 100 µL H_2O_2 (30%). Finally, the as-formed brown solution was transferred into a Teflon-lined autoclave with a capacity of 20 mL and heated for 6h at 150 °C. After the autoclave was cooled to room temperature naturally, light brown products were collected and washed with deionized water 3 times. Then the products were washed with absolute alcohol, and dried at 60 °C for 8h.

Characterization

The phase purity of the sample was examined by using a D8 Advance X-ray diffractometer with a graphite monochromater and Cu-K radiation (λ=0.15418nm). The nanostructure and morphology of the products were characterized using a transmission electron microscope (TEM, JEM 100-CX II) with an accelerating voltage of 80kV, a high-resolution transmission electron microscope (HRTEM, JEM-2100) with an accelerating voltage of 200 kV and a field-emission scanning electron microscope (FE-SEM, Hitachi, S4800). Thermogravimetric analysis (TGA) was carried out to monitor the mass loss of products at a heating rate of 10 °C min^{-1} from 25 to 800 °C under an air atmosphere (Mettler Toledo, TGA/SDTA851°). Temperature-programmed reduction under a H_2 environment (H_2-TPR) was carried out on a PCA-1200 instrument. Typically, 50 mg CeO_2 catalyst was pretreated under O_2 stream at 500 °C for 0.5 h. After cooling down to room temperature, the sample was purged with 30 mL min^{-1} of N_2 for 30 min to remove the excess O_2. Then a flow of 5% H_2-N_2 was introduced into the CeO_2 sample with a flow rate of 30 mL min^{-1} and the temperature was raised to 1000 °C at a rate of 10 °C min^{-1}. N_2 adsorption-desorption isotherms were measured on a QuadraSorb SI at 77.3K. Before the measurement, the samples were outgassed at 200 °C under vacuum for 6 h. The surface areas were calculated by the Brunauer-Emmett-Teller (BET) method, and the pore size distribution was calculated from the desorption branch using the Barrett-Joyner-Halenda (BJH) theory.

Measurement of catalytic activity

The catalytic activity of the as-obtained samples was evaluated by a continuous flow fixed-bed microreactor operating under atmospheric pressure. In a typical experiment, catalyst particles (50 mg) were placed in the reactor. Then, the samples were treated in O_2 gas with a flow rate of 30 ml/min and heated at 300 °C for 2 h. After cooling down to room temperature, the gas stream was switched to the reaction atmosphere, i.e., CO oxidation in excess O_2: 1% CO and 10% O_2 balanced with N_2, with a flow rate of 60 ml/min. The composition of the gas exiting the reactor was analyzed with an online infrared gas analyzer (Gasboard-3121, China Wuhan Cubic Co.) which simultaneously detects CO and CO_2 with a resolution of 10 ppm.

Results and discussion

Physical characterization of $Ce(HCOO)_3$ precursor

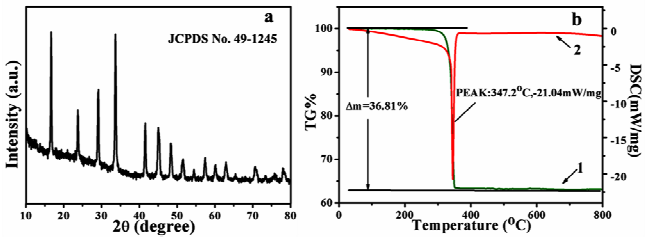

Fig. 1 (a) XRD pattern, (b1) TG, and (b2) DSC curves of the $Ce(HCOO)_3$ precursor obtained before adding H_2O_2

At the early stages of our synthesis process, a white colloidal solution was obtained immediately with the addition of the ammonia solution (10 M). The white colloids were centrifuged, dried and characterized by XRD, TGA and TEM. Fig. 1a shows the XRD pattern of the precursor, and all the diffraction peaks could be easily indexed to the rhombohedral pure phase [space group: R3 (146)] of $Ce(HCOO)_3$ (JCPDS card No. 49-1245). To investigate the thermal behavior of the $Ce(HCOO)_3$, thermogravimetry analysis was carried out under air from 30 to 800 °C with a temperature ramp of 10 °C min^{-1}. The TG curve (Fig. 1b1) indicates that the weight loss (36.81%) is approximately in agreement with the theoretical value of the conversion from $Ce(HCOO)_3$ to CeO_2.[34] Only one peak is found in the DSC curve (Fig. 1b2) during 30 to 800 °C, which is 347.2 °C. All the decomposition behaviors demonstrate that the chemical formula of the as-formed precursor is $Ce(HCOO)_3$ without crystal water.

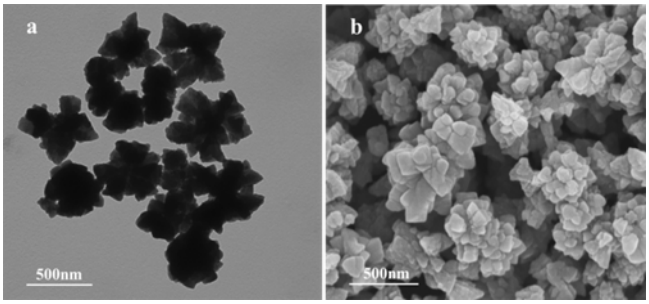

Fig. 2 Total TEM image (a) and SEM image (b) of the as-prepared $Ce(HCOO)_3$ precursor.

The size and morphology of the $Ce(HCOO)_3$ precursor were examined by transmission electron microscope (TEM) and scanning electron microscope (SEM). Fig. 2a shows a panoramic TEM image of the as-formed precursor, which indicates the nanoparticles are relatively uniform and monodisperse. It can be clearly seen from Fig. 2 that these nanoparticles are composed of many nanocones and the average diameter of these nanoparticles is about 500 nm. It is necessary to separate the nucleation from the growth for the final product with uniform size.[35] However it is hard to obtain completely uniform particles with a rapid process of nucleation and growth in an alkaline environment at room temperature, especially for 3D-hierarchical nanostructure.

Physical Characterization of CeO_2 nanoparticles

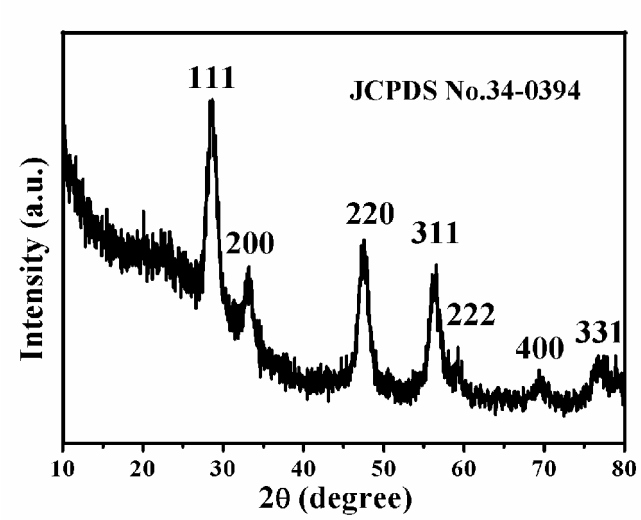

Fig. 3 XRD pattern of the CeO_2 powders after solvothermal treatment at 150 ^oC for 6h

Fig. 3 shows the typical diffraction pattern of the CeO_2 products. All diffraction peaks are in good agreement with a pure phase face-centered cubic [space group: Fm3m (225)], which is consistent with the JCPDS file of ceria (JCPDS No. 34-0394). It can be seen that there are no signals corresponding to $Ce(HCOO)_3$ in Fig. 3, indicating the high purity of the sample. Furthermore, the broadening of the peaks manifested that the sample is made up of primary small crystal particles.[36] In addition, the product obtained by annealing $Ce(HCOO)_3$ precursor is also detected by XRD (ESI, Fig. S1†) and the diffraction peaks are consistent with a pure face-centered cubic phase of ceria (JCPDS No. 34-0394).

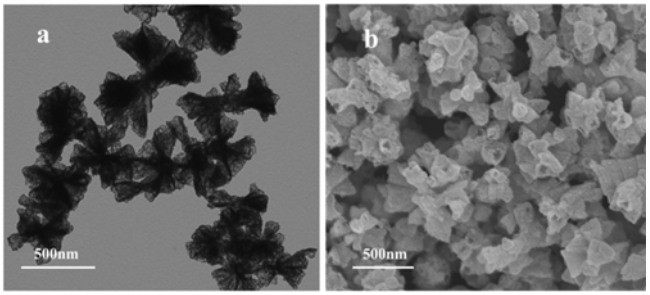

Fig. 4 Representative TEM image (a) and SEM image (b) of the CeO_2 nanoparticles

The size and morphology of the CeO_2 products were examined by transmission electron microscope (TEM) and scanning electron microscope (SEM) as shown in Fig. 4. Panoramic TEM image (Fig. 4a) and SEM image (Fig. 4b) of the CeO_2 sample show the nanoparticles with average size of 500 nm and reveal that the nanoparticle is built of several hollow nanocones. The hollow structure of these nanocones can be verified by the brightness contrast of the nanoparticles in the TEM image (Fig. 4a), which is consistent with the high-magnification SEM image (ESI, Fig. S2†). We can see from Fig. 4 that the final products not only remained the shape and dimensions of the $Ce(HCOO)_3$ template but also obtained hollow and mesoporous structure after solvothermal reaction. But the CeO_2 obtained by calcinating $Ce(HCOO)_3$ precursor did not inherit the original morphology (ESI, Fig. S3†).

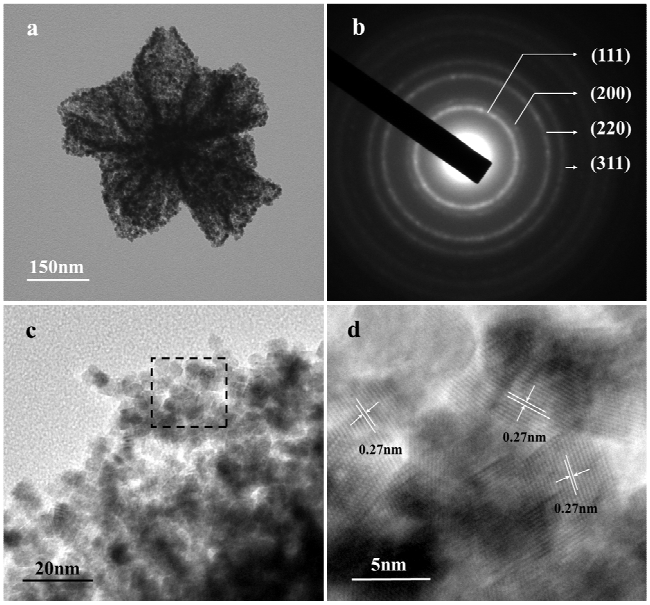

Fig. 5 TEM images of the CeO_2 products: (a) overall view of an individual nanoparticle; (b) SAED pattern of the nanoparticle; (c) a detailed view of an individual nanoparticle; (d) HRTEM images of a typical nanoparticle taken from the area marked in (c).

To identify the internal structures of nanoparticle thoroughly, more details of the nanoparticles have been investigated by the HRTEM (Fig 5). As shown in Fig 5a, the full view of a single nanoparticle indicates that the structures are made of several hollow nanocones which is in line with the high-magnification SEM image (ESI, Fig. S2†). The magnified part of a hollow nanocone (Fig 5c) confirms the nanocones are made of numerous nanocrystal particles with a crystallite size about 3-5nm. As shown in Fig. 5d, the visible lattice fringes with a spacing of about 0.27 nm clearly corresponded to the spacing of the (200) planes of ceria. Furthermore, the color contrast of the image (Fig. 5d) indicates the mesoporous structure of CeO_2 nanoparticles which is consistent with the BJH analysis. The mesoporous structure favoured for molecule accessibility to the active surface of the nanocrystals and mass transport.[37] As shown in Fig. 5b, the selected area electron diffraction (SAED) pattern of a single CeO_2 nanoparticle (Fig. 5b) indicates the typical polycrystalline nature. Therefore we could come to a conclusion that the

nanoparticles were composed of many tiny crystal particles.

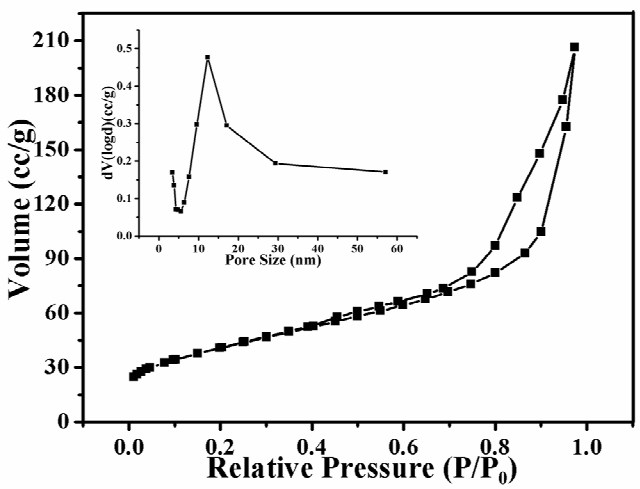

Fig. 6 N_2 adsorption-desorption isotherms of the CeO_2 nanoparticles; inset is corresponding BJH pore size distribution curve.

The textural porosities of the CeO_2 products were furthermore characterized by N_2 adsorption – desorption measurement. The N_2 adsorption – desorption isotherms are displayed in Fig. 6 and the inset part is the corresponding Barrett – Joyner – Halenda (BJH) pore size distribution plots. The obvious hysteresis loop ranging from 0.4 to 1.0 in the relative pressure suggests the existence of mesostructure in the CeO_2 nanoparticles. The calculated surface area of the CeO_2 nanoparticles is 147.6 $m^2 g^{-1}$, which is much higher than that of the commercial CeO_2 (8.5 $m^2 g^{-1}$).[38] Because the high surface area exhibits numerous crystal facets which are considered as the active sites for the adsorption of CO, the CeO_2 nanoparticles could be an ideal catalytic support for CO conversion.[31, 39] From the BJH pore size distributioin plots of the CeO_2 nanoparticles, the mesopores (5-60nm) can serve as tunnel structure for the contact between the catalytic surfaces and CO molecules.[37, 40, 41] The N_2 adsorption-desorption isotherms measurement was also used to test the calcined CeO_2 powders via cerium formate precursor (ESI, Fig. S4†) and the BET surface area of the calcined product is 114.9 $m^2 g^{-1}$.

Formation Mechanism

Based on our previous work, we used H_2O_2 as an oxidant to control the transformation from $Ce(HCOO)_3$ to CeO_2 under the protection of ammonia solution. At an early stage, a white colloidal solution was formed immediately after the addition of ammonia solution (10M) to the solution containing Ce^{3+}, H^+ and $HCOO^-$ ions. In the past research, the injection method of base is often overlooked. Herein, we find that the rapid injection method of strong ammonia (10M) is the key to obtain nano-cone constructed $Ce(HCOO)_3$ precursor. By contrast, the adhesive solid spheres (ESI, Fig. S5a†) were obtained with slow injection of strong ammonia (10M). A quick assembly process could be involved due to the fast formation of $Ce(HCOO)_3$ nanoparticles. To minimize the surface energy, the crystal growth and their interaction to form larger structures occur in geometric arrangement. This process is kinetically controlled by the preferential adsorption/desorption of anions or surfactants.[42, 43] The selectively bind of formate ions to certain crystal facets, the intrinsic crystal structure and property of the formate salts enhance the anisotropic growth to form $Ce(HCOO)_3$ nanocones.[32, 34] In a solution route, because the molecular interactions including Van der Waals forces and hydrogen bonds between capping agents benefit the interaction potentials between the particles, these nanocones organized into ordered nanoparticles spontaneously via an oriented attachment (OA) mechanism.[44, 45] In addition, the nonionic surfactant OP-10 we used here instead of PVP we frequently used before may also play a crucial role on the formation of final products due to its stabilizing behavior.[46] In the presence of PVP, CeO_2 nanoparticles assembled by solid nanocones were obtained (ESI , Fig. S5b†). The products without adding of OP-10 were also tested by TEM (ESI, Fig. S5c†).

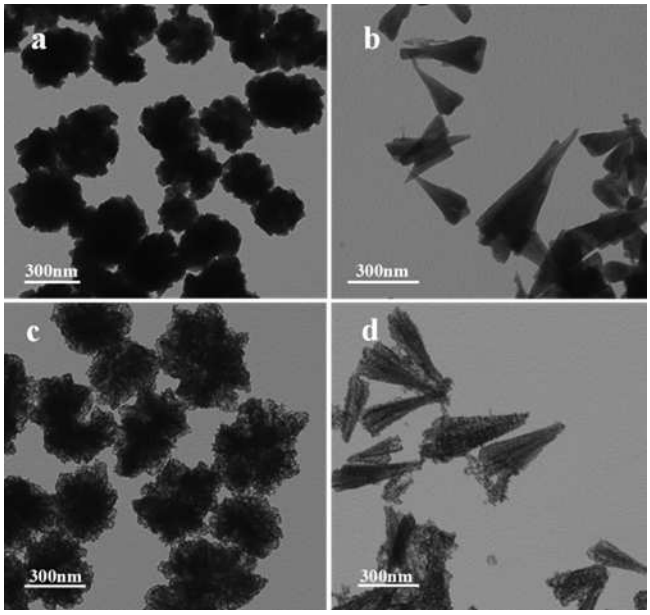

Fig. 7 The TEM images of the obtained $Ce(HCOO)_3$ precursors (a, b) and corresponding final products (c, d) when the dosage of the $NH_3 \cdot H_2O$ (10M) were 400 μL and 600 μL, respectively.

In view of the fact that the nano-cone constructed $Ce(HCOO)_3$ precursor is a hierarchical structure, we think the dosage of $NH_3 \cdot H_2O$ may have influence on nucleation and growth process of the precursor. Fig. 7 shows the TEM images of the obtained precursors and final products when the dosage of the $NH_3 \cdot H_2O$ is changed. Fig. 7a is the TEM image of the $Ce(HCOO)_3$ precursor obtained by adding 400 μL 10 M $NH_3 \cdot H_2O$ which shows that the product is consisted of solid nanospheres with rough surface. When the amount of 10 M $NH_3 \cdot H_2O$ further increased to 600 μL, dispersive cone-like nanostructure began to appear (Fig. 7b). However, the mechanism and influencing factors for the formation of the $Ce(HCOO)_3$ precursor need to be further discussed. Even though the morphology of $Ce(HCOO)_3$ was influenced by the dosage of ammonium hydroxide, we can see from Fig. 7c-d that the final products all inherited the shape and dimensions of the $Ce(HCOO)_3$ template after solvothermal reaction. Furthermore, the textural porosities of the corresponding products were tested by N_2 adsorption–desorption measurement and the BET surface area of the solid nanospheres and dispersive cone-like nanostructure are 105.7 $m^2 g^{-1}$ and 142.6 $m^2 g^{-1}$ respectively.

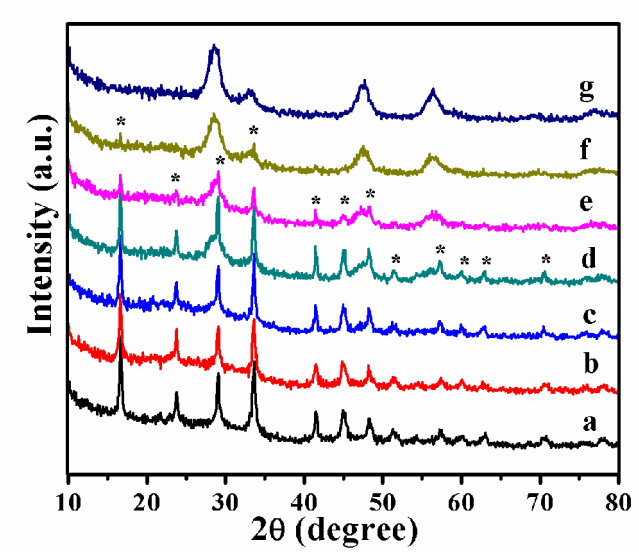

Fig. 8 XRD pattern of the products obtained after the addition ((a) ammonium solution, (b) H_2O_2) at room temperature and different solvothermal times illustrated as ((c) 20 min, (d) 40 min, (e) 1 h, (f) 2 h (g) 3 h).

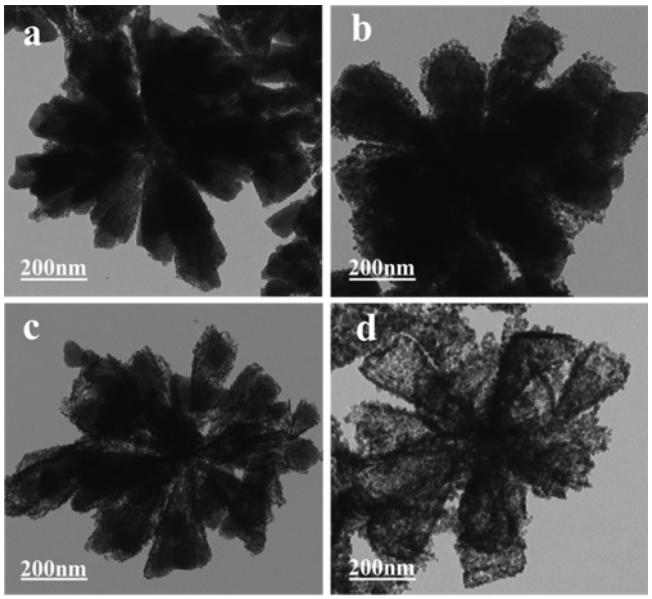

Fig. 9 The TEM images of the products obtained at differet solvothermal times illustrated as ((a) 20 min, (b) 40 min, (c) 60 min, (d) 120 min)

To get a bettter understanding of the phase transformation from $Ce(HCOO)_3$ to CeO_2 and the formation of the cone-like hollow structure, a series of time-dependent experiments were made. As shown in Fig. 8, the evolution process was examined by XRD. We obtained the TEM images of the products at different solvothermal times as shown in Fig. 9. At first, the XRD pattern (Fig. 8a) of white precipitation is well indexed to the characteristic peaks of $Ce(HCOO)_3$. The XRD pattern (Fig. 8b) of the brown precipitation after the addition of 100 μL H_2O_2 (30%) reveals that the samples were also pure phase $Ce(HCOO)_3$. After the following solvothermal treatment in the autoclave at 150 ^oC for 20 min, the $Ce(HCOO)_3$ at the surface of these nanocones had been oxidated by H_2O_2 and dissolved, but CeO_2 nuclei can not be seen from Fig. 9a. So the peaks indexed to ceria can not be seen clearly from Fig. 8c due to the absence of CeO_2 precipitation. As shown in Fig. 9b, the formed CeO_2 nuclei aggregated randomly at the surface of these noncones, and the peaks indexed to the face-centered cubic phase of ceria, such as (111) and (220), appeared as shown in Fig. 8d. Fig. 9c indicates that after 60 min solvothermal treatment, the core-shell structure formed with the dissolution of the inner $Ce(HCOO)_3$. The XRD analyses (Fig. 8e) identified the typical mixed peaks of $Ce(HCOO)_3$ (marked with *) and CeO_2 due to the remained inner $Ce(HCOO)_3$ cores and the CeO_2 shell wall. When the reaction time was prolonged to 2 h, the peaks assigned to $Ce(HCOO)_3$ almost completely disappeared, which together with Fig. 8d indicates that the transformation of $Ce(HCOO)_3$ to CeO_2 took place at this time. At the same time, the ceria nanocones with extended cavities were obtained and the inner $Ce(HCOO)_3$ cores disappeared as shown in Fig. 9d. After 3 h, the sample with a better crystallization can be observed from the XRD pattern (Fig. 8g), but no peaks of $Ce(HCOO)_3$ can be seen any more, which suggest that the phase transformation have completed.

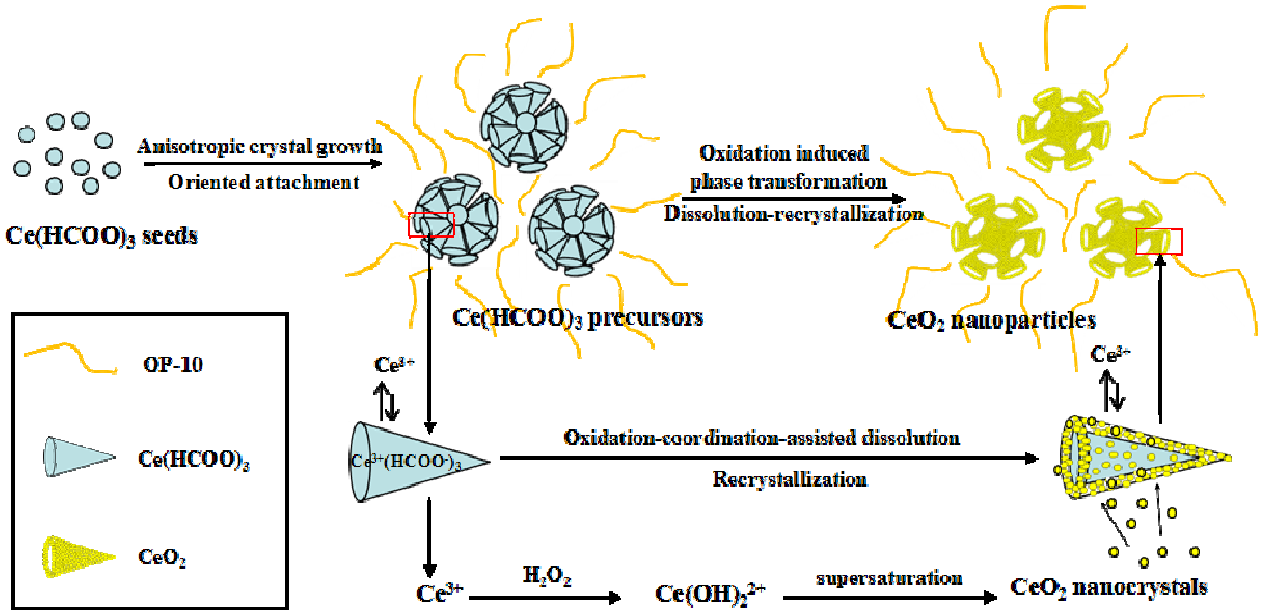

Fig. 10 The schematic illustration of the formation of mesoporous CeO_2 nanoparticles.

Based on the above XRD, TEM results and our previous work on the synthesis of flowerlike CeO_2 through an oxidation-coordination-assisted dissolution process, the phase transformation can be deduced as the following equations:

$Ce^{3+} + 3HCOOH + 3NH_3{\cdot}H_2O \rightarrow Ce(HCOO)_3 + 3NH_4^+ + 3H_2O$ (1)

$Ce(HCOO)_3(s) \rightleftarrows Ce^{3+} + 3HCOO^-$ (2)

$NH_3.H_2O \rightleftarrows NH_4^+ + OH^-$ (3)

$2Ce^{3+} + H_2O_2 + 2OH^- \rightarrow 2Ce(OH)_2^{2+}$ (4)

$Ce(OH)_2^{2+}(aq) + 2OH^- \rightarrow CeO_2(s) + 2H_2O$ (5)

The formation mechanism could be illustrated in Fig. 10. At the early stage, $Ce(HCOO)_3$ crystal seeds were generated immediately when $NH_3{\cdot}H_2O$ was added to the solution following eqn (1). In a short time, nano-cone constructed $Ce(HCOO)_3$ nanoparticles were obtained due to the anisotropic crystal growth and oriented attachment of $Ce(HCOO)_3$ crystal seeds. Then a small amount of H_2O_2 was used as oxidant which broke the dissolution-recrystallization equilibrium of $Ce(HCOO)_3$ and promoted the conversion from Ce^{3+} to Ce^{4+} complex ($Ce(OH)_2^{2+}$).[31, 39] Due to an appropriate dielectric constant of ethanol, the reaction rate of eqn (4) could be slowed down.[47] Under the alkaline environment CeO_2 was formed due to supersaturation of $Ce(OH)_2^{2+}$, thus $Ce(HCOO)_3$ was dissolved gradually with the continuous conversion of $Ce(HCOO)_3(s)$ to $Ce(OH)_2^{2+}(aq)$. Therefore, an oxidation-coordination-assisted dissolution was involved during the whole process. The formed CeO_2 nuclei would aggregate randomly at the surface of these nanocones to decrease the surface energy of the system. Meanwhile, the porous structure was formed at the outer layer of these nanocones. The porous structure at the outer layer would further provide the channels for the diffusion of the inner Ce^{3+} cation and outer H_2O_2, which ensures the complete transformation of $Ce(HCOO)_3$ to CeO_2. In the case of the partially oxidized $Ce(HCOO)_3$, since most of the outer wall had been oxidized to CeO_2 nuclei, the oxidation-coordination-assisted dissolution process continued inside the nanocones; thus, the ceria nanocones with extended cavities formed finally.[48] During this process, the amount of H_2O_2 should be controlled to avoid acceleration of the reaction (4), thus the dissolution-recrystallization process could occur slowly.

H_2-TPR Reduction Behaviors

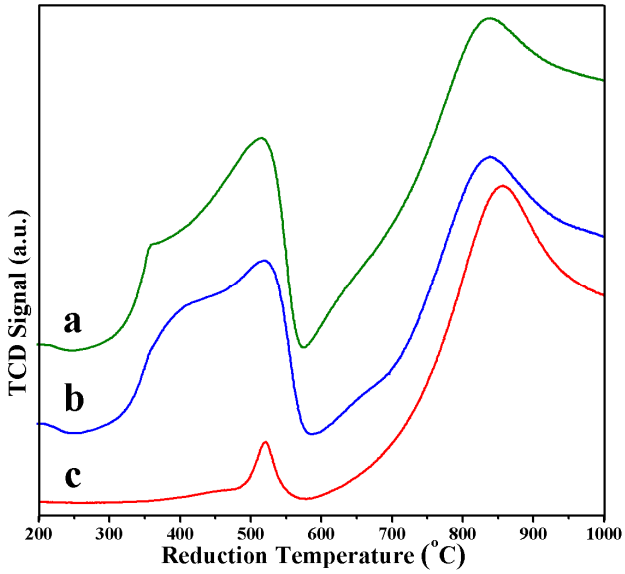

Fig. 11 H_2-TPR profiles of the as-obtained solvothermal CeO_2 nanoparticles (a), calcined spherical CeO_2 (b) and the commercial CeO_2 sample (c).

H_2-TPR tests can reveal the property of oxygen vacancies for the CeO_2 which is an important factor to affect the catalytic activity.[49] H_2-TPR measurements were performed on the as-formed hollow nano-cone constructed CeO_2 nanoparticles, the calcined CeO_2 and commercial CeO_2 samples to reveal their redox properties (Fig. 11). All samples show two major reduction peaks below 1000 °C, which are consistent with the TPR spectra

of the pure CeO_2 samples.[50] The first peak at the lower temperature (300-600 °C) is due to the reduction of the surface oxygen species or reduction of the ceria surface, while the reduction of bulk oxygen and the formation of Ce_2O_3 lead to the second peak at the higher temperature region (above 700 °C). Furthermore, there is a direct proportion relationship between the peak areas of the curves and the amount of H_2 consumption. The above three samples (a – c) based on the peak areas in TPR profiles are shown with a sequence a > b > c, which indicates the solvothermal CeO_2 sample has the best reduction behavior, followed by the calcined CeO_2 and the commercial CeO_2 sample. The more surface oxygen species due to the high surface area of the mesoporous CeO_2 nanoparticles led to the high peak area in low temperature zone which indicates the excellent catalytic property.

Catalytic properties

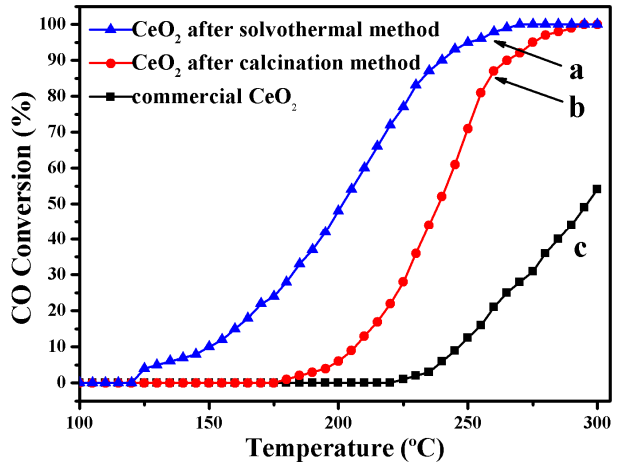

Fig. 12 Conversion of CO over (a) CeO_2 nanoparticles after solvothermal method, (b) ceria after calcination method and (c) commercial ceria

To evaluate the catalytic activity of our CeO_2 samples, the CO conversion reaction was selected as a model reaction. Fig. 12 shows the catalytic profiles of the as-obtained solvothermal CeO_2 sample along with that of the calcined CeO_2 sample and commercial CeO_2 powders for comparison. It can be seen clearly that the hollow nano-cone constructed CeO_2 sample displayed much higher catalytic activity followed by the calcined CeO_2 and then the commercial CeO_2 sample. The CO conversion of the CeO_2 nanoparticles increase rapidly with raised reaction temperature from 100 °C to 300 °C, but that of the calcined CeO_2 and commercial CeO_2 ascends slowly. For example, at 250 °C, the CO conversion is 95% for the CeO_2 sample after solvothermal method, and 71% for the calcined CeO_2 sample, while only 13% for commercial CeO_2 powders. When the CO conversion is 50%, the temperatures are about 200 °C and 245 °C for the CeO_2 sample after solvothermal and calcination method respectively. Based on our speculation, the better catalytic activity of the CeO_2 nanoparticles is attributed to the small size of the nanocrystals and high specific surface area which give many catalytically active sites, as well as the porous structures favoured for molecule accessibility to the active surface of the nanocrystals and mass transport.[37] Because the recycling performance of the catalyst is crucial to the practical applications, the catalytic tests are performed six cycles. The recycling catalytic profiles were represented and compared in Fig. S6. Obviously, the catalytic performance remains well and all the CO conversion temperature almost keep the same. The CeO_2 nanoparticles after the catalysis were collected and tested by TEM (ESI, Fig. S7†). The well retained original morphology also indicated its excellent recycling performance.

Conclusion

A one-step facile and mild solvothermal strategy was developed to synthesize hollow nano-cone constructed CeO_2 nanoparticles via a formate precursor. H_2O_2 was used as an oxidant to achieve the phase transformation from $Ce(HCOO)_3$ to CeO_2 in the solvothermal process instead of the calcination of cerium formate precursor. Oxidation-coordination-assisted dissolution-recrystallization process contributed to the formation of the hollow structure. The excellent catalytic property is attributed to the small size of the nanocrystals, high surface area and mesoporous structure of the CeO_2 nanoparticles. Because the high surface area and the porous structures, the CeO_2 nanoparticles sample can be used as not only an effective catalyst towards the conversion of CO, but aslo an ideal support material for noble metals load and the detailed studies are still under investigated. Besides, our strategy may be further extended to synthesize other metal oxides 3D hierarchical structures.

Acknowledgements

This work was supported by the Natural Science Foundation of China (grant nos 21276142) and the Natural Science Foundation of Shandong Province (grant nos ZR2013BM026).

Notes and references

1 F. Tian, J. Y. Xiong, H. P. Zhao, Y. L. Liu, S. Q. Xiao and R. Chen, *CrystEngComm*, 2014, DOI:10.1039/C4CEOO160E.
2 Q. J. Xiang, J. G. Yu and M. Jaroniec, *Chem. Commun.*, 2011, **47**, 4532.
3 L. Wang, X. H. Zhang and K. Z. Chen, *CrystEngComm,* 2013, **15**, 4860.
4 P. W. Madhusudan, J. Zhang, B. Cheng and G. Liu, *CrystEngComm*, 2013, **15**, 231.
5 Y. J. Zheng, Z. J. Huang, C. F. Zhao, S. H. Weng, W. Zheng and X. H. Lin, *Microchim Acta*, 2013, **180**, 537.
6 K. B. Xu, R. J. Zou, W. Y. Li, Y. F. Xue, G. S. Song, Q. Liu, X. J. Liu and J. Q. Hu, *J. Mater. Chem. A*, 2013, **1**, 9107.
7 F. Gao, R. H. Jin, D. C. Zhang, Q. X. Liang, Q. Q. Ye and G. H. Liu, *Green Chem.*, 2013, **15**, 2208.
8 S. L. Zhao, H. J. Yin, L . Du, G. P. Yin, Z. Y. Tang and S. Q. Liu, *J. Mater. Chem. A*, 2014, **2**, 3719.
9 G. R. Patzke, Y. Zhou, R. Kontic and F. Conrad, *Angew. Chem. Int. Ed.*, 2011, **50**, 826.
10 X. Y. Yu, G. X. Zhang, Z. Y. Lu, J. F. Liu, X. D. Lei and X. M. Sun, *CrystEngComm*, 2014, **16**, 3935.
11 X. C. Duan, J. M. Ma, J. B. Lian and W. J. Zheng, *CrystEngComm,* 2014, **16**, 2550.
12 L. L. Li, Y. L. Cheah, Y. Ko, P. Teh, G. Wee, C. L. Wong, S. J. Peng and M. Srinivasan, *J. Mater. Chem. A*, 2013, **1**, 10935.
13 F. F. Yuan, Y. H. Ni, L. Zhang, S. M. Yuan and J. D. Wei, *J. Mater. Chem. A*, 2013, **1**, 8438.

14 F. K. Chen, J. T. Zai, M. Xu and X. F. Qian, *J. Mater. Chem. A*, 2013, **1**, 4316.
15 G. H. Tian, Y. J. Chen, W. Zhou, K. Pan, Y. Z. Dong, C. G. Tian and H. G. Fu, *J. Mater. Chem.*, 2011, **21**, 887.
16 X. G. Han, L. Li and C. Wang, *CrystEngComm*, 2012, **14,** 1939.
17 L. J. Mu, Z. Y. Zhang, L. Y. Zhang, C. D. Chen and Z. Q. Zhao, *Advanced Materials Research*, 2013, **683**, 30.
18 S. P. S. Badwal, D. Fini, F. T. Ciacchi, C. Munnings, J. A. Kimpton and J. Drennan, *J. Mater. Chem. A*, 2013, **1**, 10768.
19 N. Izu, T. Itoh, M. Nishibori, I. Matsubara and W. Shin, *Sens. Actuators. B*, 2012, **171**, 350.
20 N. M. Bahadur, F. Kurayama, T. Furusawa, M. Sato, I. A. Siddiquey, M. M. Hossain and N. Suzuki, *J. Nanopart. Res.*, 2013, **15**, 1390.
21 J. Qi, J. Chen, G. D. Li, S. X. Li, Y. Gao and Z. Y. Tang, *Energy Environ. Sci.*, 2012, **5**, 8937.
22 J. Qi, K. Zhao, G. D. Li, Y. Gao, H. J. Zhao, R. B. Yu and Z. Y. Tang, *Nanoscale*, 2014, **6**, 4072.
23 D. S. Zhang, X. J. Du, L. Y. Shi and R. H. Gao, *Dalton Trans.*, 2012, **41**, 14455
24 H. Y. Xiao, Z. H. Ai and L. Z. Zhang, *J. Phys. Chem. C*,2009, **113**, 16625.
25 R. B. Yu, L. Yan, P. Zheng, J. Chen and X. R. Xing, *J. Phys. Chem. C*, 2008, **112**, 19896.
26 R. R. Cui, W. C. Lu, L. M. Zhang, B. H. Yue and S. S. Shen, *J. Phys. Chem. C*, 2009, **113**, 21520.
27 S. L. Zhong, M. Y. Wang, L. Wang, Y. Li, H. M. Nob and J. H. Jeong, CrystEngComm, 2013, DOI: 10.1039/C3CE41996G.
28 C. W. Sun, J. Sun, G. L. Xiao, H. R. Zhang, X. P. Qiu, H. Li and L. Q. Chen, *J. Phys. Chem. B*, 2006, **110**, 13445.
26 D. M. Kempaiah, S. Yin and T. Sato, *CrystEngComm*, 2011, **13**, 741.
30 J. J. Wei, Z. J. Yang and Y. Z. Yang, *CrystEngComm*, 2011, **13**, 2418.
31 J. J. Wei, Z. J. Yang, H. X. Yang, T. Sun and Y. Z. Yang, *CrystEngComm*, 2011, **13**, 4950.
32 W. Liu, L. J. Feng, C. Zhang, H. X. Yang, J. X. Guo, X. F. Liu, X. Y. Zhang and Y. Z. Yang, *J. Mater. Chem. A*, 2013, **1**, 6942.
33 X. F. Liu, H. X.Yang, L. Han, W. Liu, C. Zhang, X.Y. Zhang, S. P. Wang and Y. Z. Yang, *CrystEngComm*, 2013, **15**, 7769.
34 W. J. Shan, X. W. Dong, N. Ma, S. Y. Yao and Z. C. Feng, *Catal Lett*, 2009, **131**, 350.
35 D. S. Zhang, X. J. Du, L. Y. Shi and R. H. Gao, *Dalton Trans.*, 2012, **41**, 14455.
36 X. Liang, X. Wang, Y. Zhuang, B. Xu, S. M. Kuang and Y. D. Li, *J. Am. Chem. Soc.*, 2008, **130**, 2736.
37 J. W. Xiao, L. Wan, X. Wang, Q. Kuang, S. Dong, F. Xiao and S. Wang, *J. Mater. Chem. A*, 2014, **2**, 3794.
38 Z. J. Yang, D. Q. Han, D. L. Ma, H. Liang, L. Liu ang Y. Z. Yang, *Cryst. Growth Des.*, 2010, **10**, 291.
39 P. K. Stoimenov, V. Zaikovski and K. J. Klabunde, *J. Am. Chem. Soc.*, 2003, **125**, 12907.
40 X. W. Liu, K. B. Zhou, L. Wang, B. Y. Wang ang Y. D. Li, *J. Am. Chem. Soc.*, 2009, **131**, 3140.
41 M. A. Gabal, S. A. K. Elroby and A. Y. Obaid, *Powder Technol.*, 2012, **229**, 112.
42 S. K. Meher and G. R. Rao, *ACS Catal.*, 2012, **2**, 2795.
43 Y. W. Jun, J. S. Choi and J. Cheon, *Angew. Chem. Int. Ed.*, 2006, **45**, 3414.
44 Z. H. Li, R. Li, T. C. Mu and Y. X. Luan, *Chem. Eur. J.*, 2013, **19**, 6005.
45 R. K. Mallavajula and L. A. Archer, *Angew. Chem. Int. Ed.*, 2011, **50**, 578.
46 Z. X. Cheng, X. B. Dong, Q. Y. Pan, J. C. Zhang and X. W. Dong, *Materials Letters*, 2006, **60**, 3137.
47 R. Si, Y. W. Zhang, L. P. You and C. H. Yan, *J. Phys. Chem. B*, 2006, **110**, 5994.
48 K. B. Zhou, Z. Q. Yang and S. Yang, *Chem. Mater.*, 2007, **19**, 1215.
49 J. Ke, J. W. Xiao, W. Zhu, H. C. Liu, R. Si, Y. W. Zhang and C. H. Yan, *J. Am. Chem. Soc.*, 2013, **135**, 15191.
50 Z. L. Zhang, D. Han, S. J. Wei and Y. X. Zhang, *J. Catal.*, 2010, **276**, 16.